Journal of Catalysis 447 (2025) 116102

Contents lists available at ScienceDirect

Journal of Catalysis

journal homepage: www.elsevier.com/locate/jcat

Research Article

Adsorption properties of crystalline and amorphous PdIr nanoparticles. A systematic first-principles study

Ilya V. Chepkasov [a,b,*], Viktor S. Baidyshev [a], Anastasiia V. Iosimovska [a], Ivan S. Zamulin [b], Alexander G. Kvashnin [a]

[a] Skolkovo Institute of Science and Technology, Bolshoy Boulevard 30, bld. 1, Moscow, 121205, Russian Federation
[b] Katanov Khakas State University, 90 Lenin pr., Abakan, 655017, Russian Federation

ARTICLE INFO

Keywords:
DFT
Ab initio
IrPd
Core–shell
Amorphous nanoparticles

ABSTRACT

The great interest in metal nanoparticles is due to the fact that the transition from micro to nano size leads to huge changes in the physical and chemical properties of the material. The local atomic structure and composition can significantly influence the properties of nanoparticles. First-principles calculations are used to study the influence of the structure and chemical ordering of IrPd nanoparticles on the electronic properties, charge distribution and adsorption energy of O, H, CO, NO, OH. Three different types of PdIr bimetallic nanoparticles with different chemical ordering are considered, namely Pd-core/Ir-shell (Pd@Ir), Ir-core/Pd-shell (Ir@Pd) and bimetallic alloy (Pd-Ir) particles consisting of 79 and 321 atoms with fcc and amorphous structures. The electronic and adsorption properties of the proposed nanoparticles are extensively studied in terms of their ability to adsorb O, H, CO, NO, OH, which opens up the possibility of fine-tuning their properties by modifying the atomic structure and composition. By adjusting the core–shell ratio, the adsorption energy on the nanoparticle surface can be fine-tuned, especially in fcc nanoparticles. This results in a narrower range of adsorption energies, which cannot be achieved with bimetallic alloys. In the case of amorphous nanoparticles, the adsorption energy is highly variable because there are many non-equivalent adsorption sites on the surface.

1. Introduction

The great interest of researchers in metal nanoparticles (NPs) over the last few decades is due to the fact that the transition from the micro- to the nanoscale leads to huge changes in the physical and chemical properties of the material. The small size of the particles is one of the key features, as it leads to an increase in the surface-to-volume ratio and the emergence of quantum effects that are not present in conventional materials. These effects make metal nanoparticles promising candidates for use in catalytic applications. Palladium-iridium (PdIr) nanoalloys are considered to be important catalysts among metal nanoclusters in a number of vital applications [1–12]. For example, Pd-Ir nanoalloys act as catalysts for a number of organic reactions [13]. They are also used in preferential CO oxidation to remove impurities in H_2 production [2]. In addition, PdIr alloys can be used as multifunctional electrocatalysts in various reactions. In particular, it has been shown that PdIr nanomaterials act as bifunctional electrocatalysts for oxygen evolution reaction (OER), hydrogen evolution reaction (HER) [14] and oxygen reduction reaction (ORR) [15]. The surface composition is crucial for the different catalytic reactions, especially, since Pd shows excellent activity for hydrogen adsorption, the Ir sites can be used for hydrogen oxidation [16]. On the other hand, the Ir-rich surface of the PdIr-based electrocatalysts shows significant advantages in terms of OER activity [17–19].

For nanocatalysts, the geometrical structure is crucial for understanding their catalytic properties, since activity and selectivity depend on the structure. In particular, several descriptors have been developed to predict the adsorption properties of metals and alloys, such as the generalized coordination number [20], the orbitalwise coordination number [21], as well as trained models that predict the adsorption energy with good accuracy both on monometallic nanocatalysts and on bimetallic [22] and high-entropy alloys [23]. However, the accuracy of such approaches is only suitable for large-scale screening of desired catalyst compositions and is poorly suited for detailed studies of nanocatalyst properties. In particular, studies of changes in the adsorption properties of nanocatalysts with degradation of their structure and the appearance of new adsorption sites not previously present in the catalyst.

A number of studies have been carried out on the structure of PdIr nanoparticles with different chemical ordering, namely core–shell, Janus and bimetallic alloys [24–26]. However, previous studies have

* Corresponding author at: Skolkovo Institute of Science and Technology, Bolshoy Boulevard 30, bld. 1, Moscow, 121205, Russian Federation.
E-mail address: I.Chepkasov@skoltech.ru (I.V. Chepkasov).

https://doi.org/10.1016/j.jcat.2025.116102
Received 14 November 2024; Received in revised form 19 March 2025; Accepted 22 March 2025
Available online 3 April 2025

focused exclusively on the crystalline structure. But nanoparticles used in high-temperature catalysis can change their crystalline structure to amorphous [27–32]. Recent studies of nanocatalysts have also shown that amorphization can be considered a promising way to improve catalytic properties, as amorphous particles have a greater variety of different active sites for reactions [33–41].

In this study we consider PdIr bimetallic nanoparticles with different chemical ordering, namely Pd-core/Ir-shell (Pd@Ir), Ir-core/Pd-shell (Ir@Pd) and bimetallic alloy (Pd-Ir) particles to determine the influence of atomic structure on surface properties, i.e. electronic structure and charge. Core–shell and bimetallic alloy PdIr NPs with diameters of ∼ 1 nm (79 atoms) and ∼ 2 nm (321 atoms) with fcc and amorphous structures are considered. In the case of fcc $PdIr_{321}$ the adsorption energies of O, H, OH, CO, NO are calculated to determine the influence of the local atomic environment of PdIr NPs on the adsorption properties of the NPs. In the case of $PdIr_{79}$ with fcc and amorphous structures, the adsorption energy of O, H, OH, CO, NO at each symmetrically non-equivalent site on the surface of the nanoparticles calculated in order to determine the influence of the structure (fcc and amorphous) on the adsorption energy.

2. Computational methodology

To analyze the electronic structure and surface charge of nanoparticles using density functional theory (DFT) [42,43], we first optimize the geometry of each studied nanoparticle. The Generalized Gradient Approximation (GGA) is used with the revised PBE [44] parametrization for the exchange–correlation functional as implemented in the VASP software package [45–47]. The ion-electron interaction is described by the projector-augmented-wave (PAW) method [48] with a cut-off energy of 480 eV. The orbital occupancies are smeared using the first-order Methfessel-Paxton method with a smearing width of 0.05 eV. The local geometry optimization of the considered clusters is performed until the maximum force on each atom becomes less than 0.03 eV/Å. The nanoparticles are placed in a box with a vacuum of at least 10 Åseparating them.

The spin-polarized Generalized Gradient Approximation (GGA) with the PBE parametrization is used to calculate the adsorption energies. The Grimme correction (DFT-D3) [49] is applied to account for the dispersive van der Waals interaction. The results of the calculations are post-processed and visualized using the Open Visualization Tool (OVITO) [50] and the VESTA package [51,52]. Electron transfer is studied using the Bader analysis [53]. To determine the structural stability, the excess energy [54] of nanoparticles with respect to a bulk is calculated as follows:

$$\Delta = (E_{NPs} - E_{Ir}N_{Ir} - E_{Pd}N_{Pd})/(N_{Ir} + N_{Pd})^{2/3}, \quad (1)$$

where E_{NPs} is the energy of the considered nanoparticle, N_{Ir} and N_{Pd} correspond to the number of Pd and Ir atoms, respectively, and E_{Ir} and E_{Pd} are the energies per atom for the bulk Pd and Ir respectively.

The adsorption energies of O, H, OH, CO, NO are calculated using the following formula:

$$E_{ads}[A] = E[A/Ir_xPd_y] - E[Ir_xPd_y] - E[A], \quad (2)$$

where $E[A/Ir_xPd_y]$ are the energies of adsorption of a complex A = O, H, OH, CO, NO on Ir_xPd_y nanoparticles, $E[Ir_xPd_y]$ is the energy of the considered Ir_xPd_y nanoparticles, $E[A]$ is the energy of the gas phase OH, CO and NO molecules. For the adsorption of O and H the energy of gas phase A_2 molecule is calculated as $E[A] = \frac{1}{2}E[A_2]$, where A = O, H.

3. Results and discussion

Our study is devoted to the identification of features associated with the influence of structural type, local atomic environment, composition and chemical ordering of PdIr nanoparticles on their surface properties, including adsorption properties. We consider core–shell and bimetallic alloy PdIr nanoparticles of two sizes ∼ 1 nm (79 atoms) and ∼ 2 nm (321 atoms), with fcc and amorphous structures. For core–shell Pd@Ir and Ir@Pd nanoparticles with a size of 2 nm (321 atoms), only compositions where the entire surface consists of Ir or Pd atoms are considered. We chose three cases of core–shell nanoparticles with 55, 87, 135 atoms in the core and 266, 234, 186 atoms in the shell for fcc NPs and 57, 98, 123 atoms in the core and 264, 223, 198 atoms in the shell for amorphous NPs, see Fig. 1a,b. The different number of atoms in the core and shell for fcc and amorphous nanoparticles is due to the irregular structure of the latter. For 1 nm (79 atoms), core–shell NPs with 19 atoms in the core and 60 in the shell are considered for both fcc and amorphous structures. Amorphous nanoparticles are obtained by molecular dynamics simulation of melting of fcc PdIr nanoparticles with rapid freezing of the amorphous structure.

First, the stability of nanoparticles is studied by calculating Δ, which is the excess energy of the cluster over the bulk fragment with the same number of atoms divided approximately by the number of surface atoms in the cluster, see Eq. (1). The lower the excess energy, the more stable the nanoparticle. The dependence of Δ on the Ir concentration in Ir-Pd, Pd@Ir, and Ir@Pd nanoparticles (2 nm, 321 atoms) with both fcc and amorphous structure are shown in Fig. 1c,d. It is interesting to note that two types of core–shell nanoparticles show significantly different behavior of Δ on Ir content (red and green color in Fig. 1c,d). The Pd@Ir nanoparticles are energetically less favorable compared to other considered structures, which has also been observed previously [25,26]. This can be explained by the surface energies of Pd and Ir, determined to be 1.74 and 2.65 J/m^2, respectively [55]. The Pd surface is more favorable than Ir leading to the stabilization of Ir@Pd nanoparticles, see red line in Fig. 1c,d. Amorphous nanoparticles have slightly higher excess energy (Δ) compared to fcc due to the disordered structure and different chemical ordering, but the trends observed are the same.

In order to evaluate the catalytic efficacy of nanoparticles without performing direct calculations of the adsorption of atomic and molecular agents on the surface, a number of models can be used to determine the reactivity of nanoparticles [56,57]. For example the *d*-band model proposed by Hammer and Nørskov [56] substantiates the reactivity of transition metals based on the center of the *d*-band of surface atoms. The *d*-band model provides an accurate representation of the variation in adsorption energy for atoms and molecules at different sites on the surface of nanoparticles [20].

For all considered $PdIr_{321}$ nanoparticles, the *d*-band centers are determined by calculating the electronic density of states projected onto each atom (pDOS). The distribution of the *d*-band centers of the surface atoms for the considered $PdIr_{321}$ nanoparticles is shown in Fig. 2. It is clear that for amorphous nanoparticles the distribution of *d*-band centers is wider than for fcc nanoparticles (orange and green color, respectively, in Fig. 2). Width of distribution of *d*-band centers of surface atoms for fcc and amorphous nanoparticles $PdIr_{321}$ shown in Fig. S6 (see Supporting Information). Such a wide distribution of *d*-band center of surface atoms in amorphous nanoparticles is associated with surface disorder, where all sites on the surface are symmetrically inequivalent due to different chemical ordering compared to fcc structure. Considering nanoparticles Pd_{321}, Ir_{321} together with core–shell nanoparticles with fcc structure (green color in Fig. 2), one can see distinct peaks of *d*-band center of surface atoms. This is due to the fact that the structure is symmetrical and ordered with only a few types of symmetrically inequivalent sites on the surface according to the number of nearest neighbors. The wide distribution of the *d*-band center in the case of bimetallic alloy PdIr nanoparticles is due to the presence of

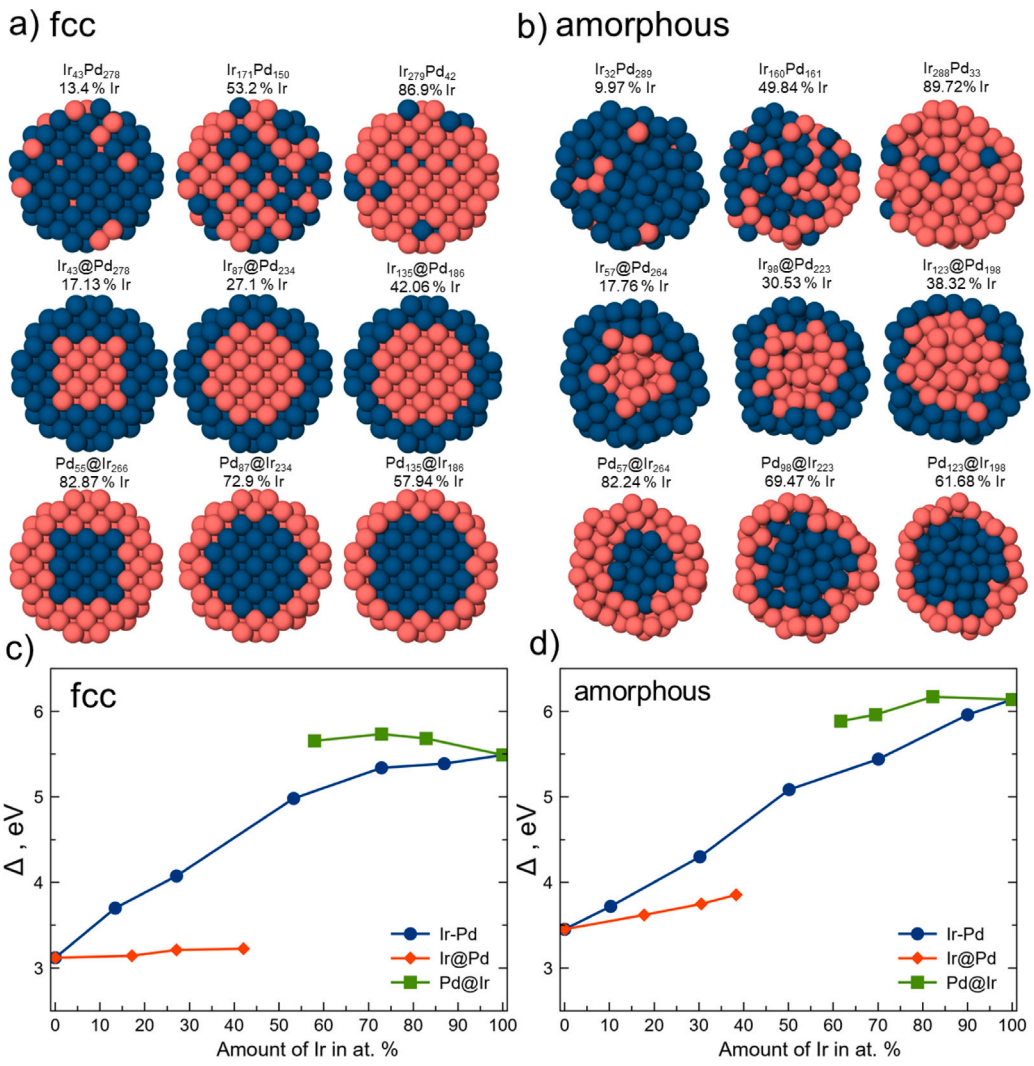

Fig. 1. (a,b) Atomic structures of the considered bimetallic fcc and amorphous $PdIr_{321}$ nanoparticles with different chemical ordering, namely the bimetallic alloys Pd-Ir, Ir@Pd, and Pd@Ir. Excess energies Δ of PdIr nanoparticles with (c) fcc and (d) amorphous structure depending on composition and chemical ordering.

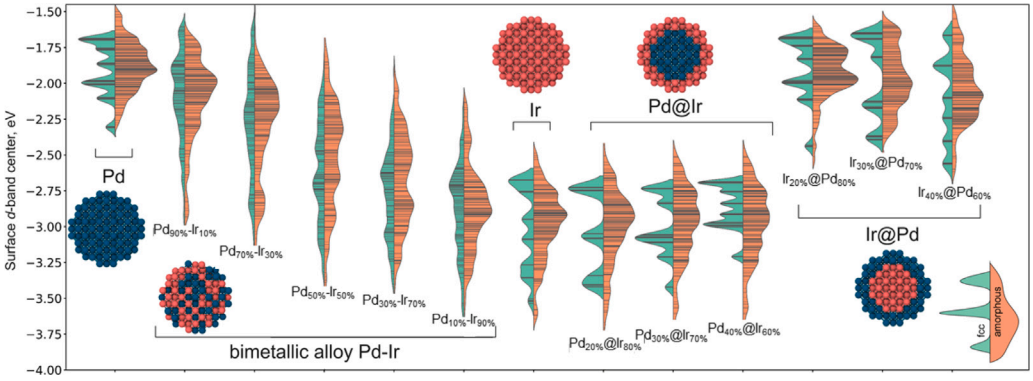

Fig. 2. Distribution of d-band centers of $PdIr_{321}$ nanoparticles with different fcc and amorphous structure depending on chemical ordering (Pd@Ir, Ir@Pd, Pd-Ir).

two types of surface atoms (Pd and Ir) with different values of the d-band center on the surface (see Fig. S5 in the Supporting Information). Analysis of the d-band center distribution for core-shell nanoparticles indicates that d-band center can be shifted by changing the core–shell size ratio. This should lead to a change in the adsorption properties of the nanoparticles [58].

Based on the distribution of d-band centers we calculate the average value among all surface atoms as shown in Fig. 3c,f. The average values of the d-band centers of the surface of pure Ir nanoparticles are −3 eV for both fcc and amorphous structure types, while for pure Pd it is −1.9 eV. Bimetallic alloy particles show a monotonic decrease in the mean value of the d-band center as a function of Ir concentration. The electronic properties of PdIr nanoparticles shift monotonically from pure Pd to pure Ir as the Ir concentration decreases. In the case of Pd@Ir (green color in Fig. 3c,f), decreasing the Ir content in the shell leads to a slight decrease in the d-band center compared to pure Ir (−3.03

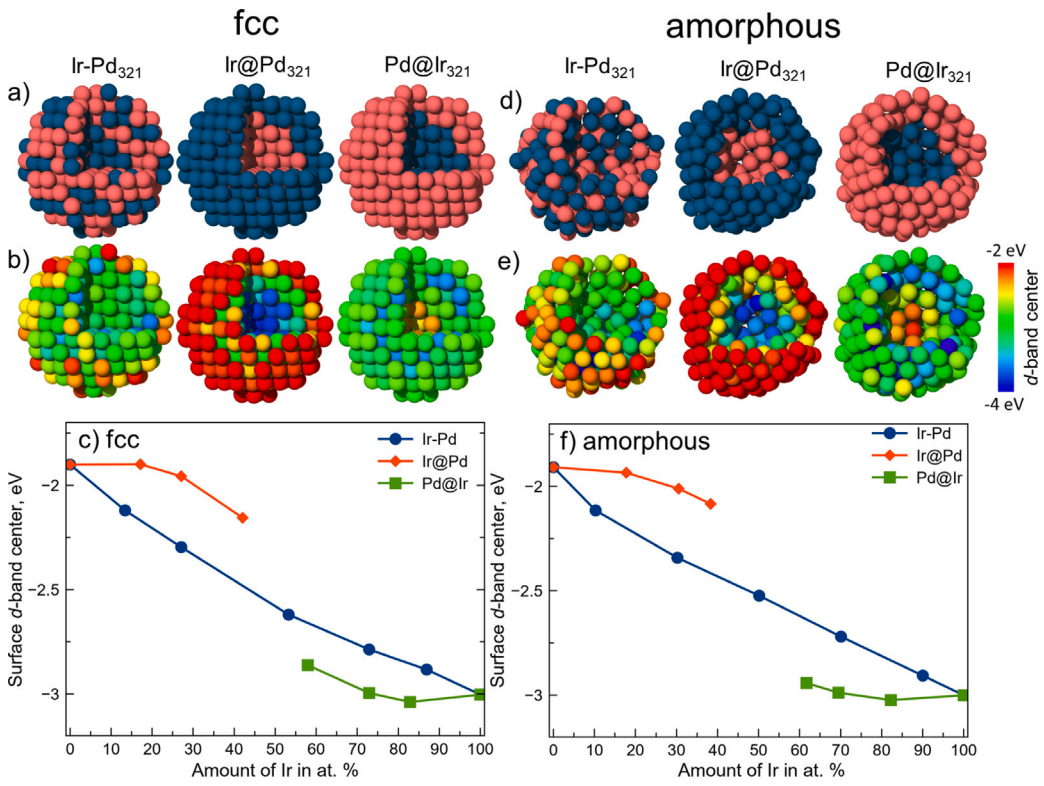

Fig. 3. (a,d) Atomic structures of bimetallic fcc and amorphous $PdIr_{321}$ nanoparticles with different chemical ordering. (b, e) Distribution of *d*-band centers. Average *d*-band centers of surface atoms calculated for nanoparticles with (c) fcc and (d) amorphous structure depending on the chemical ordering (Pd@Ir, Ir@Pd, Pd-Ir).

and −3.02 eV for fcc and amorphous respectively). Further reduction of the Ir content leads to an increase in the *d*-band center compared to pure Ir. The dependence is therefore not as monotonous as for the bimetallic alloy. For Ir@Pd (red color in Fig. 3c,f) the tendency is similar, namely an increase in the Ir content in the core leads to a slight decrease in the values of the *d*-band center. The lowering of the *d*-band center in Ir@Pd nanoparticles with a change in the core–shell ratio may lead to weakened adsorption of oxygen-containing species to promote ORR electrocatalysis [59]. Visualization of the distribution of *d*-band center values in PdIr nanoparticles depending on different structure and composition is shown in Fig. 3a,b,d,e.

One of the main factors influencing the adsorption of different chemical agents on the surface is the uncompensated surface charge resulting from the presence of broken bonds on the nanoparticle surface. Using the Bader charge analysis [53] the surface charge distribution for PdIr nanoparticles is calculated, as shown in Fig. 4. For reference the atomic structures of the considered bimetallic nanoparticles with different chemical ordering are shown in Fig. 4a,d. The distributions of atomic charges on the surfaces of nanoparticles with different structures and chemical ordering are shown in Fig. 4b,e. We observe an excess of negative charge on the surface of all considered nanoparticles (red color in Fig. 4b,e). Using these data the variation of the average surface charge is calculated as shown in Fig. 4c,f. Depending on the type of metal in the core the average surface charge changes differently with Ir content. For Ir@Pd nanoparticles the surface is more negatively charged compared to Pd@Ir, which is related to the different work functions of Pd and Ir [60]. This effect of charge redistribution in nanoparticles has been studied in detail in our previous works for the cases of PtPd, CuAu, PdAu nanoparticles [61–64].

The behavior of the surface charge and the *d*-band center as a function of composition can be explained by the variation of the shell lattice parameter depending on the core in the nanoparticle [65]. For example Guan et al. [66] used DFT to study how the lattice parameters and electronic properties of the Pt monolayer on the Au substrate (1ML-Pt/Au(111)) change. It was clearly shown that the underlying gold expands the lattice of the supported platinum layer by 4.3% from 2.77 to 2.89 Å. This lattice expansion and the orbital hybridization between platinum and gold induce a significant up-shift of the platinum *d*-band center by 0.69 eV towards the Fermi level. A shifted *d*-band center would make the exposed platinum layer more reactive. The tendency to change the interatomic distance in the shell in Au@Pd nanoparticles has also been shown previously by Zhang et al. [67]. In our work we study the change in interatomic distance on the nanoparticle surface as a function of the composition in core and shell. For Pd the interatomic distance changes from 2.725 Åfor pure Pd nanoparticles to 2.708 Åfor $Ir_{135}@Pd_{186}$ (42.06% Ir) nanoparticles. In the case of Pd@Ir nanoparticles the interatomic distance on the surface changes from 2.612 Åfor pure Ir nanoparticles to 2.645 Åfor $Pd_{135}@Ir_{186}$ (57.94% Ir) nanoparticles (see Fig. S7 in the Supporting Information). From the distribution of interatomic spacing of surface atoms in IrPd nanoparticles with fcc and amorphous structure it is well seen that the distribution is wider in amorphous particles than in fcc nanoparticles, which is due to the inhomogeneity of the structure in amorphous nanoparticles (Fig. S8 in the Supporting Information). These changes in interatomic spacing are one of the factors leading to changes in the surface properties of core–shell nanoparticles.

Considering the application of nanoparticles in catalysis, it is important to take into account the charge redistribution effect, as different molecules require different surface charges for favorable adsorption. In particular, the CO molecule prefers to bind to positively charged sites rather than negatively charged sites, due to the more pronounced nature of CO electron donation, as evidenced by previous studies [68–70]. On the other hand, it is well known that the O_2 molecule acts as an electron acceptor, strongly interacting with sites that can readily donate electrons to the antibonding orbitals of O_2 and preferentially attaching to negatively charged sites [71]. Thus, structure-driven tuning of surface charge redistribution can finely modify surface properties, opening up great prospects for their use in various applications.

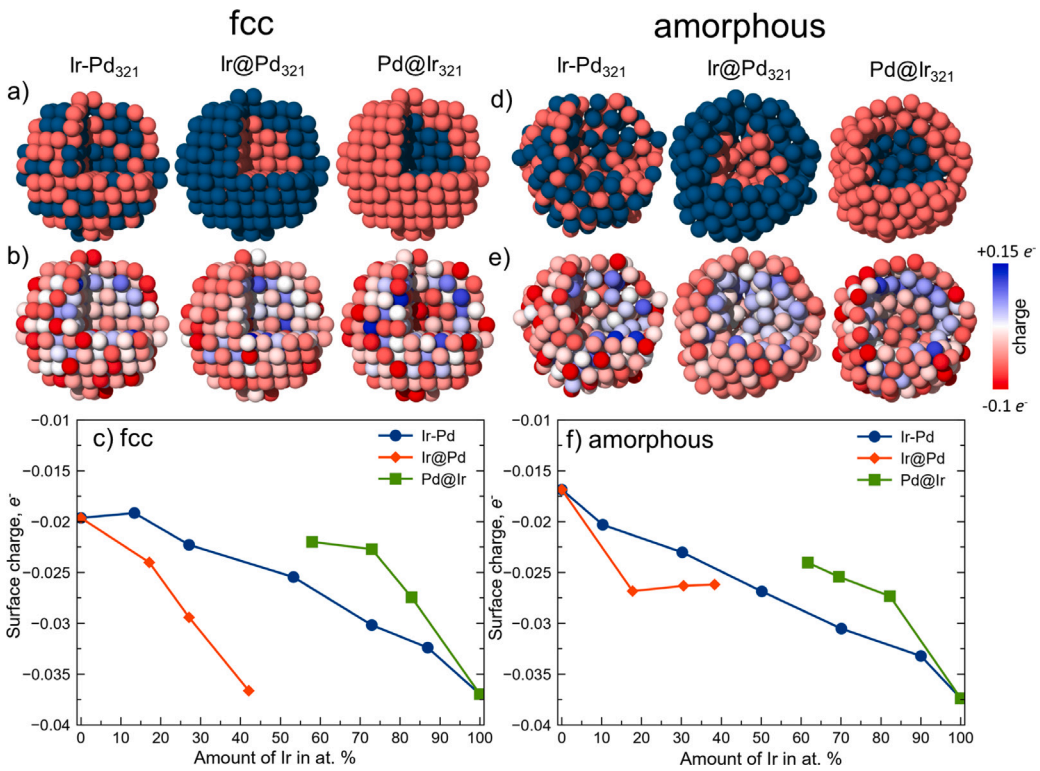

Fig. 4. (a,d) Atomic structures of bimetallic fcc and amorphous $PdIr_{321}$ nanoparticles with different chemical ordering. (b, e) Atomic charge distribution. Average surface charge in PdIr NPs with (c) fcc and (f) amorphous structure as a function of chemical ordering (Pd@Ir, Ir@Pd, Pd-Ir). Positive values of the charge indicate a deficiency of electrons (electrons have moved from the surface to the interior), negative values indicate an excess of electrons, resulting in a negative surface charge.

Since Pd-Ir nanoalloys are effectively used in oxygen evolution reaction (OER), hydrogen evolution reaction (HER) [14] and oxygen reduction reaction (ORR) [15] as well as in exhaust gas purification systems, we investigate the adsorption of products of these reactions such as O, H, CO, NO, OH on Ir-Pd nanoparticles. To study the influence of the core-to-shell thickness ratio on the adsorption properties, we chose $IrPd_{321}$ nanoparticles with fcc structure, since this particle size allows us to vary the thickness of the core and the shell. In order to determine the effect of the chemical ordering of IrPd nanoparticles on the adsorption energy of O, H, CO, NO, and OH, we consider 14 different adsorption sites on the surface of fIrPd nanoparticles with fcc structure. Different adsorption sites, including top, bridge, hollow and kink are considered to give the most complete picture of adsorption (see Supporting Information). The atomic structure of the kink adsorption site is presented in the Supporting Information. Fig. 5 shows the average values of adsorption energies O, H, CO, NO, OH on $IrPd_{321}$ core–shell and bimetallic alloy nanoparticles. The adsorption energies of O, H, CO, NO, OH on the iridium-terminated surface of Pd@Ir nanoparticles are lower than those for Ir@Pd nanoparticles with a Pd surface (Fig. 5). In all considered cases, the average adsorption energy changes with the change of the core-to-shell ratio in the particle. This effect was previously observed in the study of AuCu, AuPd nanoparticles [62–64].

In addition we consider bimetallic IrPd alloy nanoparticles with almost equal content of Ir and Pd atoms (160 atoms of Ir and 161 atoms of Pd). For the cases of H, CO, and NO, the average adsorption energies for pure Ir and Pd nanoparticles do not differ significantly from each other (Fig. 5), namely for H E_{ads} is −0.35 eV (Pd) and −0.43 eV (Ir), for CO E_{ads} −1.74 eV (Pd) and −1.80 eV (Ir), and for NO E_{ads} −2.35 eV (Pd) and −2.37 eV (Ir). A lower adsorption energy results in greater binding of the gaseous agent to the surface. Therefore, obviously that on the IrPd bimetallic alloy surface the adsorption energies do not strongly depend on the composition of the nanoparticle and the adsorption site, as can be seen in Fig. 5. On the other hand, in the case of atomic oxygen (O) and OH, the adsorption energies are very different for pure metals, in particular for O −1.09 eV (Pd) and −1.71 eV (Ir) and for OH −2.47 eV (Pd) and 2.81 eV (Ir) (Fig. 5). This implies that the adsorption energy of O and OH on the surface of the bimetallic IrPd alloy is strongly dependent on the composition of the adsorption site, i.e. the chemical ordering. Fig. 5f shows the adsorption energy of O at different sites on the surface of IrPd bimetallic alloy nanoparticles. The site consisting only of Ir atoms (site IrIr from −2.53 to 2.07 eV) binds oxygen much more strongly than the mixed IrPd sites, while the pure Pd sites have the maximum adsorption energies of −0.8 eV. For each adsorption site on each particle, we plotted the correlation of adsorption energies from different descriptors. The worst correlation is observed between the adsorption energy and the generalized coordination number. This is because this descriptor does not work for bimetallic nanoparticles and particles with a complex structure such as core–shell (Fig. S11 and Fig. S12 in the Supporting Information). The correlation between the charge and the *d*-band center at the adsorption site and the adsorption energy is not as clear (Fig. S9 and Fig. S10 in the Supporting Information). The poor correlation between the *d*-band center and the adsorption energy may be due to the fact that the adsorption site consists of several atoms, and it is necessary to take the average value of the *d*-band center of these atoms. Also a small number of adsorption sites has been chosen which is not enough to give a complete picture. Therefore, in order to study in detail the influence of the structure and composition of the nanoparticles on adsorption properties, we calculated all possible adsorption sites on $IrPd_{79}$ nanoparticles.

In order to determine the influence of the structure on the adsorption energy, we calculate the adsorption of O, H, CO, NO, and OH at each non-equivalent site on the surface of $IrPd_{79}$ nanoparticle (hollow sites for O and H, top sites for CO, NO, and OH). Pure Ir_{79} and Pd_{79} nanoparticles, bimetallic IrPd alloy ($Ir_{39}Pd_{40}$) nanoparticles and core–shell ($Ir_{19}@Pd_{60}$ or $Pd_{19}@Ir_{60}$) nanoparticles with fcc and amorphous structures are considered. The distributions of adsorption energies of O, H, CO, NO, and OH are shown in Fig. 6. These distributions for pure Ir_{79}

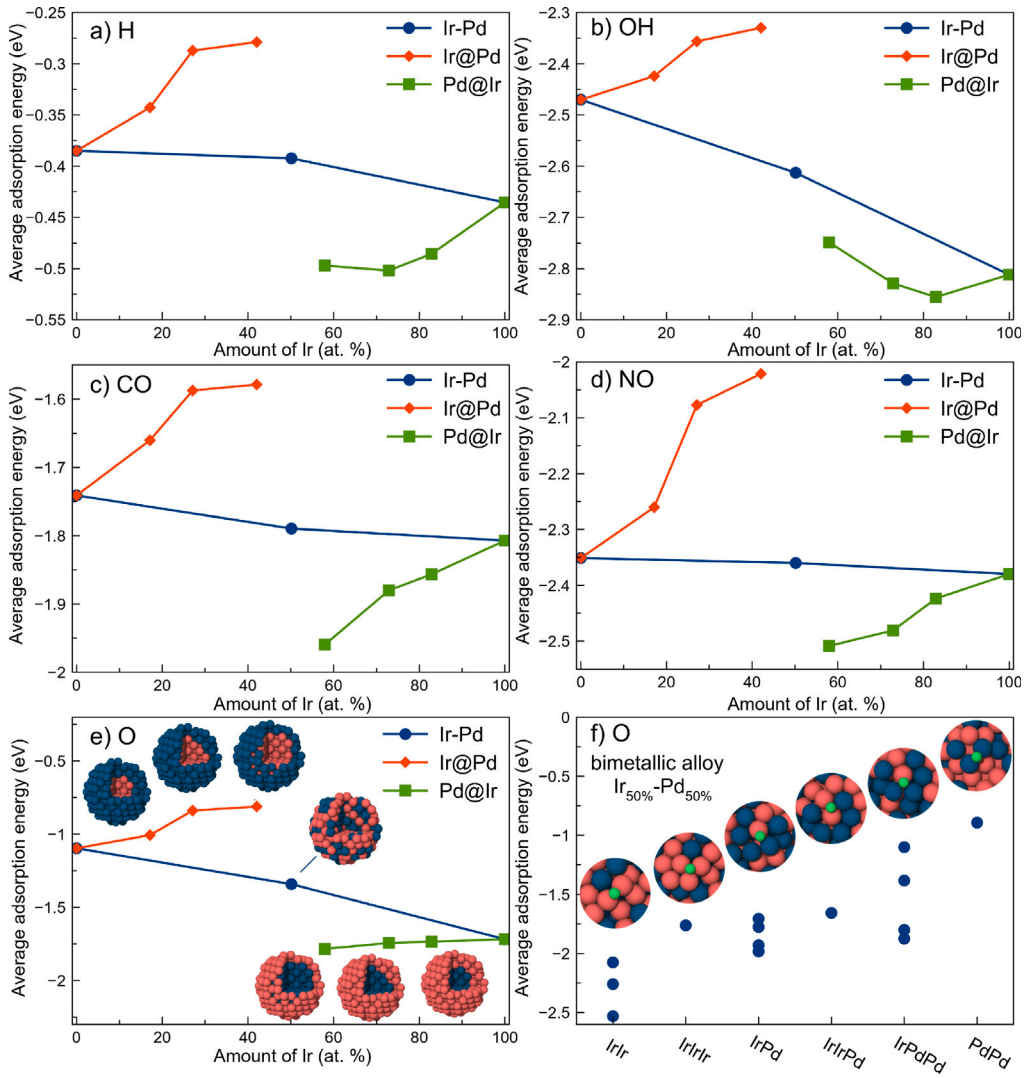

Fig. 5. Mean adsorption energy of (a) H, (b) OH, (c) CO, (d) NO and (e) CO on $IrPd_{321}$ with different chemical ordering (Ir@Pd, Pd@Ir, Ir-Pd). (f) Binding energies of O atoms on the considered bimetallic Ir-Pd alloy (50% Ir, 50% Pd) nanoparticles for different compositions and adsorption sites.

and Pd_{79} nanoparticles with fcc structure have several distinct peaks depending on the adsorption site. In particular, for the adsorption of CO on Pd_{79}, these peaks are located at −1.24 and −1.53 eV, while forthe adsorption on Ir_{79} they are −2.08, −2.28 and −2.48 eV. These values are in good agreement with the adsorption energies of CO on Ir_{79} and Pd_{79} nanoparticles obtained by Fan et al. [25]. In the case of bimetallic fcc nanoparticles, the adsorption energy distribution does not have such clear peaks because the adsorption energy is strongly dependent on the composition of the adsorption site. For core–shell nanoparticles, the adsorption energy distribution also has clear peaks, but these peaks are slightly shifted compared to pure Ir and Pd nanoparticles due to the change in surface properties in core–shell nanoparticles discussed earlier. Similar to Fan et al. [25], our calculations show that the adsorption energies of all considered atomic and molecular groups on Pd@Ir nanoparticles are lower than those on Ir@Pd nanoparticles. In particular, Pd@Ir particles have the two largest peaks on the CO adsorption energy distribution, namely at −1.38 and −1.10 eV, while Ir@Pd particles have two largest peaks at −2.29 and −2.78 eV.

The adsorption energy distributions look quite different in the case of amorphous nanoparticles. The distribution is strongly smeared because there are many more non-equivalent adsorption sites on the surface compared to fcc nanoparticles. The disordered structure is also indicated by the wide distribution of the generalized coordination number for amorphous nanoparticles compared to fcc (see Fig S12 in the Supporting Information). For example, for amorphous Ir nanoparticles, the adsorption energy varies from −0.29 to −1.87 for H and from −1.17 to −3.58 eV for oxygen, see Fig. 6a. However, the main trends in adsorption energy variation are in response to chemical ordering, i.e. the composition of core and shell in core–shell nanoparticles (Pd@Ir or Ir@Pd), but the adsorption energy distribution is more smeared. The change in catalytic activity upon amorphization has previously been demonstrates for iridium oxides. In particular, it has been shown [72–75] that amorphous iridium oxides usually exhibit higher OER catalytic activity than pure metallic iridium or crystalline iridium oxide such as rutile. It has been shown that amorphous IrO_x catalysts have abundant electronic defects and unsaturated coordination on the surface caused by a large number of randomly oriented bonds. The disordered atomic arrangement helps to improve the exposure of active sites. The flexible structure allows the catalyst to self-adjust the geometry during the reaction process to increase the number of active species and change the atomic coordination [76]. Pd-based amorphous nanoparticles also exhibit enhanced oxygen reduction reaction (ORR) activity and durability compared to their crystalline counterparts [77]. Thus, the change in adsorption properties of amorphous IrPd nanoparticles of different structures shown in this work may be important for the design of IrPd-based catalysts.

We have also studied the effect of CO and NO coverage of two types (Ir@Pd and Pd@Ir) of core–shell nanoparticles. Heterogeneous catalysis

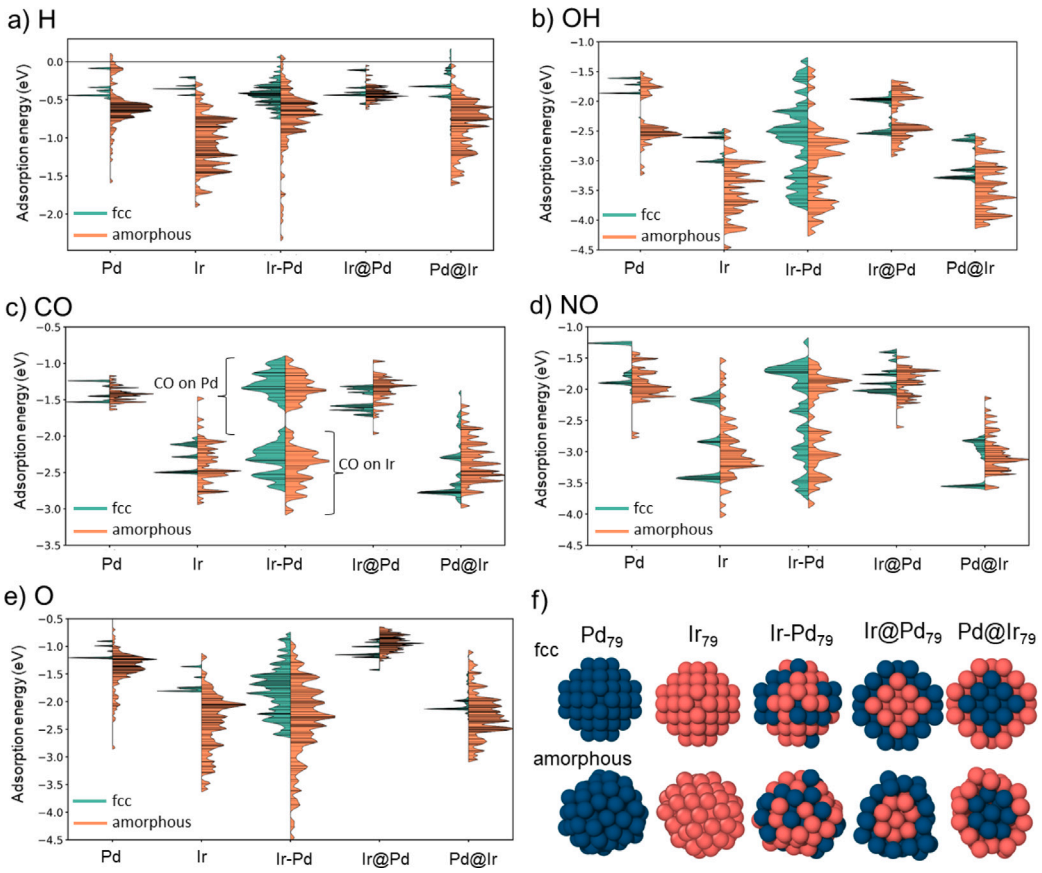

Fig. 6. Distribution of adsorption energy for (a) H, (b) OH, (c) CO, (d) NO and (e) O on $IrPd_{79}$ with fcc and amorphous structure. (f) Atomic structures of the considered fcc and amorphous nanoparticles.

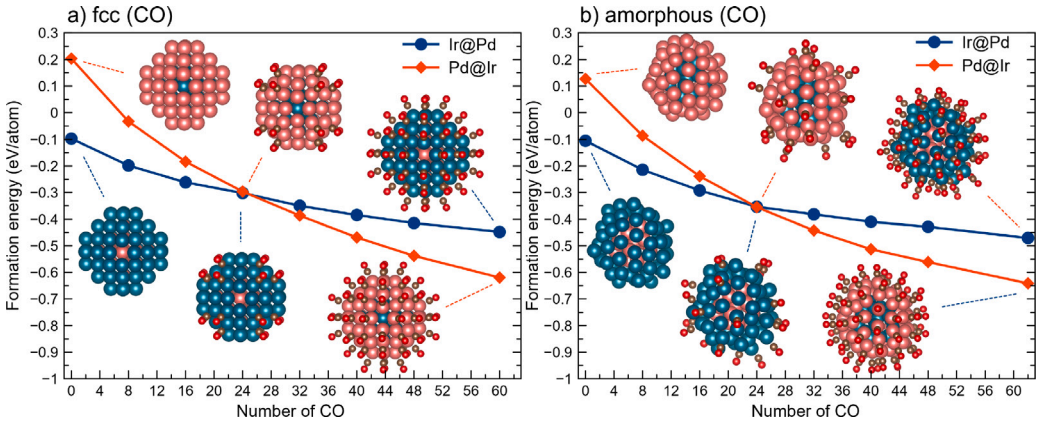

Fig. 7. Formation energy as a function of CO concentration on surface of $IrPd_{79}$ nanoparticles with different chemical ordering (Ir@Pd, Pd@Ir) and structure (fcc and amorphous).

requires the presence of reacring species on the catalyst surface, the amount of which depends on the temperature and pressure of the reaction. The concentration of surface species is known to significantly affect the properties of the catalyst in some reactions [78,79]. For example, CO is an abundant surface species in such important reactions as thermal or electrochemical CO and CO_2 reduction reactions and CO oxidation [80,81]. The presence of a significant number of CO molecules on the surface of Cu nanoparticles leds to profound changes in the electronic structure, as was shown by Kozlov et al. [82]. This has a profound effect on the catalytic properties of Cu particles in an exemplary reaction of CO dimerization into OCCO. Neyman et al. [83] showed that CO coverage of Pd-Au alloy nanoparticles leads to the fact that increasing CO concentration on the surface induces segregation of Pd on the surface, although without CO the most energetically favorable structure was Pd-core/Au-shell. The driving force for such structural reconstruction is a strong interaction of surface Pd sites with adsorbed CO molecules, which changes the surface energy, making surface segregation of Pd with formation of Pd_x-CO units energetically favorable. Nanba et al. [84] showed that NO coating of Pd-Ru alloy nanoparticles leads to the fact that increasing NO concentration on the surface makes Pd-core/Ru-shell nanoparticles most energetically favorable, although without NO molecules on the surface the Pd-core/Ru-shell structure was energetically unfavorable compared to others. This is because the adsorption on Ru sites was stronger than that on Pd sites. The energy gain due to NO adsorption outweighed the energy loss due to Pd-Ru bonds and the placement of Ru atoms on the surface. The above

examples show that adsorption of CO or NO molecules can significantly change the structure of bimetallic nanoparticles.

To study the effect of CO and NO molecules on the Pd@Ir and Ir@Pd nanoparticles with fcc and amorphous structures, the formation energy (more details in the Supporting Information) is calculated with different numbers of CO and NO molecules on surface. Without CO or NO molecules, the formation energy of the Ir-core/Pd-shell type of nanoparticles was 0.3 eV for fcc and 0.23 for amorphous more favorable than for the Pd-core/Ir-shell type. When the number of CO molecules on the nanoparticle surface increases up to 24, a transition occurs and the Pd@Ir particle becomes more energetically favorable (Fig. 7). When fully covered by CO molecules the formation energy of Pd-core/Ir-shell type of nanoparticles was 0.17 eV more favorable for fcc and for amorphous than for Ir-core/Pd-shell type. The same pattern is observed for NO (see Supporting Information). This effect is due to the fact that the adsorption energy of CO and NO is higher on Ir sites than on Pd sites. This is due to the fact that the adsorption energy of CO and NO on Pd@Ir nanoparticles is lower than on Ir@Pd nanoparticles (Fig. 6 c,d), which makes Pd@Ir particles more energetically favorable when the number of CO or NO molecules on the nanoparticle surface increases. This should be taken into account when using Ir-Pd nanoparticles in industrial reactions.

4. Conclusions

Here we have studied the influence of composition (Ir:Pd ratio), structure type (fcc or amorphous) and local atomic environment (core–shell and alloy) of bimetallic IrPd nanoparticles with a diameter of 2 nm (321 atoms) on the electronic properties and charge distribution. It is found that the type of core–shell nanoparticles (Ir@Pd and Pd@Ir) together with the thickness of the shell with respect to the core drastically affects the surface charge. Nanoparticles in which the Ir core is covered by an atomic-thick Pd shell (Ir@Pd) show a significant excess of electrons flowing from the Ir core to the Pd surface, forming a negative charge on the surface. At the same time, the structure type (fcc or amorphous) of the core–shell nanoparticles has almost no effect on the surface charge. For alloy nanoparticles, the surface charge is independent of changes in all properties (composition, local atomic environment, and structure type). The calculated *d*-band center for all considered nanoparticles shows their great potential for catalysis. The lowering of the *d*-band center in Ir@Pd nanoparticles with a change in the core–shell ratio may indicate that it weakens the adsorption of oxygen-containing species to promote ORR electrocatalysis. The adsorption of O, H, CO, NO, OH on the surface of $IrPd_{321}$ nanoparticles with fcc structure type is studied in terms of changes in the core-to-shell ratio. The adsorption energies of O, H, CO, NO, OH on the iridium-terminated surface of Pd@Ir nanoparticles are lower than those of Ir@Pd nanoparticles with Pd surface. In order to determine the influence of nanoparticle structure and chemical ordering on the adsorption energy, the adsorption of O, H, CO, NO, and OH at each non-equivalent site on the surface of $IrPd_{79}$ nanoparticles (pure, core–shell and bimetallic alloy) with fcc and amorphous structure is calculated. The distribution of adsorption energies of O, H, CO, NO, and OH on fcc $IrPd_{79}$ has several distinct peaks depending on the adsorption site. On the other hand, in the case of amorphous $IrPd_{79}$ nanoparticles, the distribution is strongly smeared because there are many non-equivalent adsorption sites on the surface. Amorphization of the catalyst can lead to an increase in catalytic activity, for example, in the OER, due to the abundance of electronic defects and unsaturated coordination on the surface caused by a large number of randomly oriented bonds. The Pd@Ir structure becomes more energetically favorable than Ir@Pd when covered with NO or CO, although it is more favorable without molecules on the Ir@Pd surface. The results of this study open up great prospects for tuning the catalytic properties of nanocatalysts by modifying their local atomic environment and structure.

CRediT authorship contribution statement

Ilya V. Chepkasov: Writing – review & editing, Writing – original draft, Visualization, Investigation, Formal analysis, Data curation, Conceptualization. **Viktor S. Baidyshev:** Visualization, Investigation. **Anastasiia V. Iosimovska:** Visualization. **Ivan S. Zamulin:** Investigation. **Alexander G. Kvashnin:** Writing – review & editing, Writing – original draft, Supervision, Investigation, Conceptualization.

Declaration of competing interest

The authors declare that they have no known competing financial interests or personal relationships that could have appeared to influence the work reported in this paper.

Acknowledgment

The research was carried out using resources of the Center for the Information and Computing of Novosibirsk State University and Zhores supercomputer of Skoltech.

Appendix A. Supplementary data

Supplementary material related to this article can be found online at https://doi.org/10.1016/j.jcat.2025.116102.

Data availability

Data will be made available on request.

References

[1] Y.M. López-De Jesús, C.E. Johnson, J.R. Monnier, C.T. Williams, Selective hydrogenation of benzonitrile by alumina-supported Ir–Pd catalysts, Top. Catal. 53 (2010) 1132–1137.
[2] F. Morfin, S. Nassreddine, J. Rousset, L. Piccolo, Nanoalloying effect in the preferential oxidation of CO over Ir–Pd catalysts, ACS Catal. 2 (10) (2012) 2161–2168.
[3] K. Persson, A. Ersson, K. Jansson, N. Iverlund, S. Järås, Influence of co-metals on bimetallic palladium catalysts for methane combustion, J. Catalysis 231 (1) (2005) 139–150.
[4] A. Rocha, E. Moreno, G. Da Silva, J. Zotin, A. Faro Jr., Tetralin hydrogenation on dealuminated Y zeolite-supported bimetallic Pd-Ir catalysts, Catal. Today 133 (2008) 394–399.
[5] S. Shen, T. Zhao, J. Xu, Carbon-supported bimetallic PdIr catalysts for ethanol oxidation in alkaline media, Electrochim. Acta 55 (28) (2010) 9179–9184.
[6] C. Zlotea, F. Morfin, T. Nguyen, N. Nguyen, J. Nelayah, C. Ricolleau, M. Latroche, L. Piccolo, Nanoalloying bulk-immiscible iridium and palladium inhibits hydride formation and promotes catalytic performances, Nanoscale 6 (17) (2014) 9955–9959.
[7] Y. Nakagawa, K. Takada, M. Tamura, K. Tomishige, Total hydrogenation of furfural and 5-hydroxymethylfurfural over supported Pd–Ir alloy catalyst, ACS Catal. 4 (8) (2014) 2718–2726.
[8] H. Yang, C. Huang, F. Yang, X. Yang, L. Du, S. Liao, Mesoporous silica nanoparticle supported PdIr bimetal catalyst for selective hydrogenation, and the significant promotional effect of Ir, Appl. Surf. Sci. 357 (2015) 558–563.
[9] M. Liu, Y. Zheng, S. Xie, N. Li, N. Lu, J. Wang, M.J. Kim, L. Guo, Y. Xia, Facile synthesis of Pd–Ir bimetallic octapods and nanocages through galvanic replacement and co-reduction, and their use for hydrazine decomposition, Phys. Chem. Chem. Phys. 15 (28) (2013) 11822–11829.
[10] X. Xia, L. Figueroa-Cosme, J. Tao, H.-C. Peng, G. Niu, Y. Zhu, Y. Xia, Facile synthesis of iridium nanocrystals with well-controlled facets using seed-mediated growth, J. Am. Chem. Soc. 136 (31) (2014) 10878–10881.
[11] M. Assumpção, S. Da Silva, R. De Souza, G. Buzzo, E. Spinacé, M. Santos, A. Neto, J. Silva, Investigation of PdIr/C electrocatalysts as anode on the performance of direct ammonia fuel cell, J. Power Sources 268 (2014) 129–136.
[12] T. Yang, Y. Ma, Q. Huang, G. Cao, Palladium–iridium nanocrystals for enhancement of electrocatalytic activity toward oxygen reduction reaction, Nano Energy 19 (2016) 257–268.
[13] L. Piccolo, S. Nassreddine, M. Aouine, C. Ulhaq, C. Geantet, Supported Ir–Pd nanoalloys: Size–composition correlation and consequences on tetralin hydroconversion properties, J. Catalysis 292 (2012) 173–180.

[14] A. Yang, T. Li, S. Jiang, X. Wang, X. Qiu, W. Lei, Y. Tang, High-density growth of ultrafine PdIr nanowires on graphene: reducing the graphene wrinkles and serving as efficient bifunctional electrocatalysts for water splitting, Nanoscale 11 (31) (2019) 14561–14568.
[15] A.T.N. Nguyen, J.H. Shim, Facile one-step synthesis of Ir-Pd bimetallic alloy networks as efficient bifunctional catalysts for oxygen reduction and oxygen evolution reactions, J. Electroanal. Chem. 827 (2018) 120–127.
[16] D.W. Flaherty, Direct synthesis of H2O2 from H2 and O2 on Pd catalysts: current understanding, outstanding questions, and research needs, ACS Catal. 8 (2) (2018) 1520–1527.
[17] T. Zhang, S.-A. Liao, L.-X. Dai, J.-W. Yu, W. Zhu, Y.-W. Zhang, Ir-Pd nanoalloys with enhanced surface-microstructure-sensitive catalytic activity for oxygen evolution reaction in acidic and alkaline media, Sci. China Mater 61 (7) (2018) 926–938.
[18] J. Zhu, Z. Chen, M. Xie, Z. Lyu, M. Chi, M. Mavrikakis, W. Jin, Y. Xia, Iridium-based cubic nanocages with 1.1-nm-Thick walls: A highly efficient and durable electrocatalyst for water oxidation in an acidic medium, Angew. Chem. 131 (22) (2019) 7322–7326.
[19] J. Zhu, Z. Lyu, Z. Chen, M. Xie, M. Chi, W. Jin, Y. Xia, Facile synthesis and characterization of Pd@ Ir n L (n=1–4) core–shell nanocubes for highly efficient oxygen evolution in acidic media, Chem. Mater. 31 (15) (2019) 5867–5875.
[20] F. Calle-Vallejo, J.I. Martínez, J.M. García-Lastra, P. Sautet, D. Loffreda, Fast prediction of adsorption properties for platinum nanocatalysts with generalized coordination numbers, Angew. Chem. Int. Ed. 53 (32) (2014) 8316–8319.
[21] X. Ma, H. Xin, Orbitalwise coordination number for predicting adsorption properties of metal nanocatalysts, Phys. Rev. Lett. 118 (3) (2017) 036101.
[22] J. Dean, M.G. Taylor, G. Mpourmpakis, Unfolding adsorption on metal nanoparticles: Connecting stability with catalysis, Sci. Adv. 5 (9) (2019) eaax5101.
[23] T.A. Batchelor, J.K. Pedersen, S.H. Winther, I.E. Castelli, K.W. Jacobsen, J. Rossmeisl, High-entropy alloys as a discovery platform for electrocatalysis, Joule 3 (3) (2019) 834–845.
[24] T.-E. Fan, Y.-R. Zhang, W. Jiang, A two-step optimization approach for structures investigation of Pd-Ir bimetallic nanoclusters, Comput. Mater. Sci. 214 (2022) 111680.
[25] T.-E. Fan, I. Demiroglu, H.A. Hussein, T.-D. Liu, R.L. Johnston, DFT study of the structure, chemical ordering and molecular adsorption of Pd–Ir nanoalloys, Phys. Chem. Chem. Phys. 19 (39) (2017) 27090–27098.
[26] I. Demiroglu, T.-E. Fan, Z. Li, J. Yuan, T.-D. Liu, L. Piccolo, R.L. Johnston, Modelling free and oxide-supported nanoalloy catalysts: comparison of bulk-immiscible Pd–Ir and Au–Rh systems and influence of a TiO 2 support, Faraday Discuss. 208 (2018) 53–66.
[27] Y.Y. Gafner, S. Gafner, I. Chepkasov, The effect of thermal treatment on the organization of copper and nickel nanoclusters synthesized from the gas phase, J. Exp. Theor. Phys. 111 (4) (2010) 608–618.
[28] I. Chepkasov, Y.Y. Gafner, S. Gafner, Changing of the shape and structure of cu nanoclusters generated from a gas phase: MD simulations, J. Aerosol Sci. 91 (2016) 33–42.
[29] I.V. Chepkasov, Y.Y. Gafner, M. Vysotin, L. Redel', A study of melting of various types of Pt–Pd nanoparticles, Phys. Solid State 59 (2017) 2076–2081.
[30] I. Chepkasov, Y.Y. Gafner, S. Gafner, Synthesis of Cu nanoparticles by condensation from the gas phase, Phase Transit. 90 (6) (2017) 590–597.
[31] I. Chepkasov, Y.Y. Gafner, S. Gafner, S. Bardahanov, Condensation of Cu nanoparticles from the gas phase, Phys. Met. Met. 117 (2016) 1003–1012.
[32] I. Chepkasov, Y.Y. Gafner, S. Gafner, S. Bardakhanov, The general mechanisms of Cu cluster formation in the processes of condensation from the gas phase, Bull. Mater. Sci. 38 (3) (2015) 701–706.
[33] Q. Fu, L.W. Wong, F. Zheng, X. Zheng, C.S. Tsang, K.H. Lai, W. Shen, T.H. Ly, Q. Deng, J. Zhao, Unraveling and leveraging in situ surface amorphization for enhanced hydrogen evolution reaction in alkaline media, Nat. Commun. 14 (1) (2023) 6462.
[34] X. Zhang, J. Zhang, B. Xu, K. Wang, X.W. Sun, Synergistic effects in biphasic nanostructured electrocatalyst: Crystalline core versus amorphous shell, Nano Energy 41 (2017) 788–797.
[35] Z. Lyu, J. Cai, X.-G. Zhang, H. Li, H. Huang, S. Wang, T. Li, Q. Wang, Z. Xie, S. Xie, Biphase Pd nanosheets with atomic-hybrid RhOx/Pd amorphous skins disentangle the activity-stability trade-off in oxygen reduction reaction, Adv. Mater. (2024) 2314252.
[36] Y. Zhang, L. Gao, E.J. Hensen, J.P. Hofmann, Evaluating the stability of Co2P electrocatalysts in the hydrogen evolution reaction for both acidic and alkaline electrolytes, ACS Energy Lett. 3 (6) (2018) 1360–1365.
[37] Y. Zeng, M. Zhao, Z. Huang, W. Zhu, J. Zheng, Q. Jiang, Z. Wang, H. Liang, Surface reconstruction of water splitting electrocatalysts, Adv. Energy Mater. 12 (33) (2022) 2201713.
[38] Z. Wu, L. Huang, H. Liu, H. Wang, Element-specific restructuring of anion- and cation-substituted cobalt phosphide nanoparticles under electrochemical water-splitting conditions, ACS Catal. 9 (4) (2019) 2956–2961.
[39] R. Sharma, M.A. Karlsen, P. Morgen, J. Chamier, D.B. Ravnsbæk, S.M. Andersen, Crystalline disorder, surface chemistry, and their effects on the oxygen evolution reaction (OER) activity of mass-produced nanostructured iridium oxides, ACS Appl. Energy Mater. 4 (3) (2021) 2552–2562.
[40] P. Jovanovic, N. Hodnik, F. Ruiz-Zepeda, I. Arčon, B. Jozinovic, M. Zorko, M. Bele, M. Šala, V.S. Selih, S. Hocevar, et al., Electrochemical dissolution of iridium and iridium oxide particles in acidic media: transmission electron microscopy, electrochemical flow cell coupled to inductively coupled plasma mass spectrometry, and X-ray absorption spectroscopy study, J. Am. Chem. Soc. 139 (36) (2017) 12837–12846.
[41] S. Cherevko, T. Reier, A.R. Zeradjanin, Z. Pawolek, P. Strasser, K.J. Mayrhofer, Stability of nanostructured iridium oxide electrocatalysts during oxygen evolution reaction in acidic environment, Electrochem. Commun. 48 (2014) 81–85.
[42] L.J. Sham, W. Kohn, One-particle properties of an inhomogeneous interacting electron gas, Phys. Rev. 145 (2) (1966) 561.
[43] P. Hohenberg, W. Kohn, Inhomogeneous electron gas, Phys. Rev. 136 (3B) (1964) B864.
[44] B. Hammer, L.B. Hansen, J.K. Nørskov, Improved adsorption energetics within density-functional theory using revised Perdew-Burke-Ernzerhof functionals, Phys. Rev. B 59 (11) (1999) 7413.
[45] G. Kresse, J. Hafner, Norm-conserving and ultrasoft pseudopotentials for first-row and transition elements, J. Phys.: Condens. Matter. 6 (40) (1994) 8245.
[46] G. Kresse, J. Hafner, Ab initio molecular-dynamics simulation of the liquid-metal–amorphous-semiconductor transition in germanium, Phys. Rev. B 49 (20) (1994) 14251.
[47] G. Kresse, J. Furthmüller, Efficient iterative schemes for ab initio total-energy calculations using a plane-wave basis set, Phys. Rev. B 54 (16) (1996) 11169.
[48] P.E. Blöchl, Projector augmented-wave method, Phys. Rev. B 50 (24) (1994) 17953.
[49] S. Grimme, J. Antony, S. Ehrlich, H. Krieg, A consistent and accurate ab initio parametrization of density functional dispersion correction (DFT-D) for the 94 elements H-Pu, J. Chem. Phys. 132 (15) (2010) 154104.
[50] A. Stukowski, Visualization and analysis of atomistic simulation data with OVITO–the open visualization tool, Modelling Simul. Mater. Sci. Eng. 18 (1) (2009) 015012.
[51] K. Momma, F. Izumi, VESTA: a three-dimensional visualization system for electronic and structural analysis, J. Appl. Crystallogr. 41 (3) (2008) 653–658.
[52] K. Momma, F. Izumi, VESTA 3 for three-dimensional visualization of crystal, volumetric and morphology data, J. Appl. Crystallogr. 44 (6) (2011) 1272–1276.
[53] W. Tang, E. Sanville, G. Henkelman, A grid-based Bader analysis algorithm without lattice bias, J. Phys.: Condens. Matter. 21 (8) (2009) 084204.
[54] R. Ferrando, G. Rossi, A.C. Levi, Z. Kuntová, F. Nita, A. Jelea, C. Mottet, G. Barcaro, A. Fortunelli, J. Goniakowski, Structures of metal nanoparticles adsorbed on MgO (001). I. Ag and Au, J. Chem. Phys. 130 (17) (2009).
[55] W. Tyson, W. Miller, Surface free energies of solid metals: Estimation from liquid surface tension measurements, Surf. Sci. 62 (1) (1977) 267–276.
[56] B. Hammer, J.K. Nørskov, Theoretical surface science and catalysis—calculations and concepts, in: Advances in Catalysis, vol. 45, Elsevier, 2000, pp. 71–129.
[57] S. Zha, Z.-J. Zhao, S. Chen, S. Liu, T. Liu, F. Studt, J. Gong, Predicting the catalytic activity of surface oxidation reactions by ionization energies, CCS Chem. 2 (4) (2020) 262–270.
[58] S. Jiao, X. Fu, H. Huang, Descriptors for the evaluation of electrocatalytic reactions: d-Band theory and beyond, Adv. Funct. Mater. 32 (4) (2022) 2107651.
[59] F. Lin, F. Lv, Q. Zhang, H. Luo, K. Wang, J. Zhou, W. Zhang, W. Zhang, D. Wang, L. Gu, S. Guo, Local coordination regulation through tuning atomic-scale cavities of Pd metallene toward efficient oxygen reduction electrocatalysis, Adv. Mater. 34 (27) (2022) 2202084.
[60] W.M. Haynes, CRC Handbook of Chemistry and Physics, CRC Press, 2016.
[61] I. Chepkasov, M. Visotin, E. Kovaleva, A. Manakhov, V. Baidyshev, Z. Popov, Stability and electronic properties of PtPd nanoparticles via MD and DFT calculations, J. Phys. Chem. C 122 (31) (2018) 18070–18076.
[62] I.V. Chepkasov, V.S. Baidyshev, A.A. Golubnichiy, I.S. Zamulin, A.G. Kvashnin, S.M. Kozlov, Cu–au nanoparticles produced by the aggregation of gas-phase metal atoms for CO oxidation: Special issue: Emerging investigators, Aggregate 3 (6) (2022) e273.
[63] I.V. Chepkasov, V.S. Baidyshev, A.G. Kvashnin, Structure-driven tuning of O and CO adsorption on AuCu nanoparticles: A density functional theory study, Phys. Rev. B 108 (20) (2023) 205414.
[64] I.V. Chepkasov, I.S. Zamulin, V.S. Baidyshev, A.G. Kvashnin, Tuning the surface properties of AuPd nanoparticles for adsorption of O and CO, Phys. Chem. Chem. Phys. 25 (48) (2023) 33031–33037.
[65] I.V. Chepkasov, A.D. Radina, A.G. Kvashnin, Structure-driven tuning of catalytic properties of core–shell nanostructures, Nanoscale 16 (2024) 5870–5892.
[66] Q. Guan, C. Zhu, Y. Lin, E.I. Vovk, X. Zhou, Y. Yang, H. Yu, L. Cao, H. Wang, X. Zhang, et al., Bimetallic monolayer catalyst breaks the activity–selectivity trade-off on metal particle size for efficient chemoselective hydrogenations, Nat. Catal. 4 (10) (2021) 840–849.
[67] X. Zhang, Z. Sun, R. Jin, C. Zhu, C. Zhao, Y. Lin, Q. Guan, L. Cao, H. Wang, S. Li, et al., Conjugated dual size effect of core-shell particles synergizes bimetallic catalysis, Nat. Commun. 14 (1) (2023) 530.
[68] X.-N. Li, Z. Yuan, S.-G. He, CO oxidation promoted by gold atoms supported on titanium oxide cluster anions, J. Am. Chem. Soc. 136 (9) (2014) 3617–3623.
[69] J.-J. Chen, X.-N. Li, Q. Chen, Q.-Y. Liu, L.-X. Jiang, S.-G. He, Neutral Au1-doped cluster catalysts AuTi2O3–6 for CO oxidation by O2, J. Am. Chem. Soc. 141 (5) (2018) 2027–2034.

[70] A.D. Radina, V.S. Baidyshev, I.V. Chepkasov, N.A. Matsokin, T. Altalhi, B.I. Yakobson, A.G. Kvashnin, Theoretical study of adsorption properties and CO oxidation reaction on surfaces of higher tungsten boride, Sci. Rep. 14 (1) (2024) 12788.
[71] M.A. Dar, S. Krishnamurty, Molecular and dissociative adsorption of oxygen on Au–Pd bimetallic clusters: Role of composition and spin state of the cluster, ACS Omega 4 (7) (2019) 12687–12695.
[72] J. Gao, C.-Q. Xu, S.-F. Hung, W. Liu, W. Cai, Z. Zeng, C. Jia, H.M. Chen, H. Xiao, J. Li, et al., Breaking long-range order in iridium oxide by alkali ion for efficient water oxidation, J. Am. Chem. Soc. 141 (7) (2019) 3014–3023.
[73] B. Jiang, J. Kim, Y. Guo, K.C. Wu, S.M. Alshehri, T. Ahamad, N. Alhokbany, J. Henzie, Y. Yamachi, Efficient oxygen evolution on mesoporous IrO x nanosheets, Catal. Sci. Technol. 9 (14) (2019) 3697–3702.
[74] M. Du, Y. Meng, G. Zhu, M. Gao, H.-Y. Hsu, F. Liu, Intrinsic electrocatalytic activity of a single IrO x nanoparticle towards oxygen evolution reaction, Nanoscale 12 (43) (2020) 22014–22021.
[75] M.E.C. Pascuzzi, J.P. Hofmann, E.J. Hensen, Promoting oxygen evolution of IrO2 in acid electrolyte by Mn, Electrochim. Acta 366 (2021) 137448.
[76] S. Zhang, X. Ma, Y. He, Y. Zhu, Z. Wang, Amorphous mixed Ir–Mn oxide catalysts for the oxygen evolution reaction in PEM water electrolysis for H2 production, Int. J. Hydrog. Energy 48 (28) (2023) 10532–10544.
[77] Z. Yu, Y. Chen, J. Xia, Q. Yao, Z. Hu, W.-H. Huang, C.-W. Pao, W. Hu, X.-M. Meng, L.-M. Yang, et al., Amorphization activated multimetallic Pd alloys for boosting oxygen reduction catalysis, Nano Lett. 24 (4) (2024) 1205–1213.
[78] H.A. Aleksandrov, S.M. Kozlov, G.N. Vayssilov, K.M. Neyman, Approaching complexity of alkyl hydrogenation on Pd via density-functional modelling, Phys. Chem. Chem. Phys. 19 (32) (2017) 21514–21521.
[79] C. Guo, Y. Mao, Z. Yao, J. Chen, P. Hu, Examination of the key issues in microkinetics: CO oxidation on Rh (1 1 1), J. Catalysis 379 (2019) 52–59.
[80] B. Sun, M. Dai, S. Cai, H. Cheng, K. Song, Y. Yu, H. Hu, Challenges and strategies towards copper-based catalysts for enhanced electrochemical CO2 reduction to multi-carbon products, Fuel 332 (2023) 126114.
[81] Y. Cao, R. Ran, X. Wu, Z. Si, F. Kang, D. Weng, Progress on metal-support interactions in Pd-based catalysts for automobile emission control, J. Environ. Sci. 125 (2023) 401–426.
[82] P.C. Mendes, U. Anjum, W. Lin, E.M. Smith, S.M. Kozlov, CO dimerization on Cu nanoparticles under high CO coverage, Ind. Eng. Chem. Res. 62 (47) (2023) 20107–20115.
[83] M. Mamatkulov, I.V. Yudanov, A.V. Bukhtiyarov, I.P. Prosvirin, V.I. Bukhtiyarov, K.M. Neyman, Pd segregation on the surface of bimetallic PdAu nanoparticles induced by low coverage of adsorbed CO, J. Phys. Chem. C 123 (13) (2018) 8037–8046.
[84] Y. Nanba, M. Haneda, M. Koyama, Facilitation of Pd–Ru mixing in nanoalloys of immiscible palladium and ruthenium by NO adsorption, J. Phys. Chem. C 128 (36) (2024) 14937–14946.